Thesis for the degree of Licentiate of Engineering

# Simulation and assessment of particle transport in fusion plasmas

Emil Fransson


CHALMERS
UNIVERSITY OF TECHNOLOGY

Department of Space Earth and Environment
*Division of Astronomy and Plasma Physics*
Chalmers University of Technology
Gothenburg, Sweden 2021

# Simulation and assessment of particle transport in fusion plasmas

Emil Fransson



Division of Astronomy and Plasma Physics
Department of Space Earth and Environment
Chalmers University of Technology
SE-412 96 Gothenburg
Telephone +46 31 772 1000

**Contact information:**
Emil Fransson
Hörsalsvägen 11
Chalmers University of Technology
SE–412 58 Gothenburg, Sweden

Phone: +46 (0)31 772 15 67
Email: emil.fransson@chalmers.se

Printed by Chalmers Reproservice
Gothenburg, Sweden 2021

# Simulation and assessment of particle transport in fusion plasmas

Emil Fransson
Department of Space Earth and Environment
Chalmers University of Technology

# Abstract

A civilized society need energy to function. An attractive new energy source is nuclear fusion with its abundance of fuel, intrinsic safety and limited environmental impact. Although the concept of fusion for energy has been well understood for over a century, to create it here on earth has been more irksome. The most developed concept for fusion is the tokamak, which is a torodial shaped chamber where a hot ionized gas, a plasma, is confined with a strong magnetic field. Early concepts showed promising results, however later machines showed much larger transport than was expected, this was due to turbulent transport.
The plasma can be described in a number of different ways, fluid or kinetic descriptions. As the particles are confined to the magnetic field lines due to Lorentz force and this process, called gyromotion, is one of the fastest process in the plasma, it is beneficial to average out this motion. This is the basis of gyrofluid and gyrokinetic descriptions. Several different codes have been devolved such as EDWM, TGLF and GENE etc from the fluid, gyrofluid and gyrokinetic descriptions. All these describes the different instabilities which dominates the plasma: the Ion Temperature Gradient (ITG), Trapped Electron Mode (TEM) and Electron Temperature Gradient (ETG).
After introducing the aforementioned descriptions of the plasma we discuss the density peaking of the plasma as it important for the efficiency of a commercial fusion power plant.

Keywords: Fusion – Plasma physics – Turbulent transport –Gyrofluid –Gyrokinetic

# Research Contributions

This thesis is based on the work contained in the following papers:

I F Eriksson, E Fransson, M Oberparleiter, H Nordman1, P Strand, A Salmi, T Tala and JET Contributors:
*Interpretative and predictive modelling of JET collisionality scans*
Plasma Phys. Control. Fusion **61**, 102487 (2019)

II T. Tala, H. Nordman, A. Salmi, C. Bourdelle, J. Citrin, A. Czarnecka, F. Eriksson, E. Fransson, C. Giroud, J. Hillesheim, C. Maggi, P. Mantica, A. Mariani, M. Maslov, L. Meneses, S. Menmuir, S. Mordijck, V. Naulin, M. Oberparleiter, G. Sips, D. Tegnered, M. Tsalas, H. Weisen and JET Contributors:
*Density Peaking in JET - Driven by Fuelling or Transport?*
Nucl. Fusion **59**, 126030 (2019)

III S. Mordijck, T.L. Rhodes, L. Zeng, A. Salmi, T. Tala, C.C. Petty, G.R. McKee, R. Reksoatmodjo, F. Eriksson, E. Fransson and H. Nordman:
*Collisionality driven turbulent particle transport changes in DIII-D H-mode plasmas*
Nucl. Fusion **60**, 066019 (2020)

IV E. Fransson, F. Eriksson, M. Oberparleiter, M. Held, S. Mordijck, H. Nordman, A. Salmi, P. Strand1, T. Tala and JET contributors:
*Comparing particle transport in JET and DIII-D plasmas: gyrokinetic and gyrofluid modelling*
Nucl. Fusion **61**, 016015 (2021)

# Acknowledgements

First, I would like to thank my supervisors Pär Strand, Hans Nordman and Michael Oberparleiter. Hans has taught me the theoretical jungle that plasma physics sometimes can be. Michael has explained with patience and kindness the numerical frameworks. Pär has tried to throw a bit of both at me to see if something sticks. I would also like to thank my colleagues at the Plasma Physics group for making it an inspiring and fun workplace. I have thoroughly enjoyed working with every single one of my colleagues during my time at Chalmers. I also send my regard to my colleagues at SEE which I have been fortunately to come cross during my years here. Lastly but certainly not least I would like to thank August, Algot, Iris and Adeline for inspiring me.

Emil Fransson, Gothenburg, February 2021

*Education is an admirable thing, but it is well to remember from time to time that nothing that is worth knowing can be taught.*
*~ Oscar Wilde*

# CONTENTS

# CHAPTER 1

# INTRODUCTION

The sun has always had a special place in human history, first as a God then as the center of the solar system but always as a source of warmth and energy. To emulate this, as it seemed, infinite energy source have been a dream for humans for eons and have been an ongoing field of research for the past decades.

## 1.1 Fusion

The energy from the sun is produced by nuclear fusion which is the process of two lighter elements fusing together into a heavier one. This process yields excess energy for all nucleus lighter than iron, due to the binding energy of the nucleus. The binding energy per nuclei is displayed in Figure (1.1), and the highest binding energy is for iron, Fe.

In a similar fashion if we split an element heavier than iron we release energy as well, this process is called fission. Fission is usually done with a neutron as the instigator. A major disadvantage with fusion is that both nuclei are positive charged and the nuclei need large kinetic energy to overcome the Coulomb repulsion.

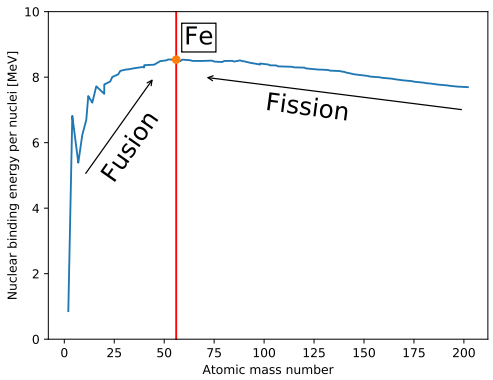


**Figure 1.1:** *Binding energy*

To achieve nuclear fusion energy here on earth the fuisonable material need to be contained together. This is done in the stars by the means of gravitation, which is obviously not an option on earth. The fusion process in the stars begins with the fusion of two protons. This process is however not suitable for a fusion power plant on earth due to the low cross section. It is different processes that are the most promising, specifically the ones between two Deuterium nuclei and Deuterium and Tritium.

$$D + D \rightarrow He^3 + n + 3.27\ MeV \tag{1.1a}$$
$$D + D \rightarrow T + H + 4.05\ MeV \tag{1.1b}$$
$$D + T \rightarrow He^4 + n + 17.58\ MeV \tag{1.1c}$$

An important thing to notice about these processes is that they do not create any radioactive waste product as $He^4$ is a stable isotop. The reaction rate of these processes are govern by their cross sections. The cross sections for these processes are shown in Figure (1.2). We can notice that the cross section is much higher for D+T than for D+D, therefore the former process is the one that the scientific community is pressing towards. However, this process have some drawbacks as Tritium is an unstable hydrogen isotope and has a half-life of 12.3 years. A result of this is that the isotope is extremely rare in nature and hard to store. A solution to this is that fusion power plants should produce their own Tritium. This can be done by bombarding Lithium with a neutron, and the resulting reaction creates a Tritium isotope according to (1.2b).

$$Li^6 + n \rightarrow T + He^4 + 4.8\ MeV \tag{1.2a}$$
$$Li^7 + n \rightarrow T + He^4 + n - 2.5\ MeV \tag{1.2b}$$

This is the reason that future fusion power plants will have Lithium blanket which will breed Tritium. There is estimated 80 million tons of lithium in the world and with a conversion rate of 0.86 GWy/ton in a fusion power plant there is enough Lithium to fuel the worlds current energy demand for 4000 years. This time can be considerably shorter if Lithium is used in other applications (lithium is a key component in today's batteries). However, there is a large amount of Lithium in the worlds oceans, billions of tons. The other fuel source for the fusion process, Deuterium is luckily much more accessible as it can be procured by extracting it from heavy water through electrolysis. Heavy water can be extracted from fresh water. Since it is extracted from water the deuterium reserves are vast, 1 part in 6400 in water. As the fuel for a pure Deuterium-fueled power plant is much more accessible the hope is that a Deuterium power plant might someday work. But the first logical step (and easiest) is to create a D-T fusion power plant. As D-T is the fuel for a power plant it seemed prudent to use this in experiments. However, the experiments with D-T are rare and long in between due to the high number of energetic neutrons these experiments create. These neutrons activate the tokamak walls and they become radioactive, hence a neutron count for each experiment is a vital part to take into to consideration when designing experiments. Therefore most

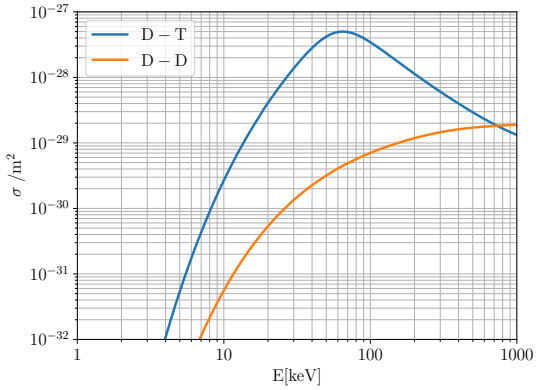


**Figure 1.2:** *Cross section for D-D and D-T reactions*

.

experiments today are run with hydrogen, deuterium and sometimes with Helium. Even though this is a different fuel composition from a future power plant these plasmas display similar behavior as a D-T plasma.

A major advantage for fusion reactors compared to fission reactors are that they are intrinsically safe. The maximum energy that can be released in an accident is the total energy stored in the reactor at a time. In a fusion reactor only a small amount of energy is contained at the same time (the total mass of the fuel is about the same as that of a stamp) and when it's operational it need a continuing stream of new nuclei to sustain power production. If one stops the flow of new nuclei the plasma will quickly cool.

## 1.2 Different approaches to fusion

There are three main fields of research trying to obtain fusion power production, inertial confinement fusion, stellarators and tokamaks. Inertial confinement fusion uses the same principle as a hydrogen bomb, which sounds hazardous however the amount of fusionable material is so small it is a safe process. The material is heated and compressed extremely quickly so that it reaches the sufficient condition for fusion. The material is held together by the inertia of the fuel itself, hence the name. The fuel is prepared in a small pellet with a radius of a few millimeters and put in a so called hohlraum. There it is bombarded by high energetic laser beams that compress the pellet. As the pellet is compressed instabilities can occur and the fusion criteria might not be achieved. This is an ongoing field of research and relies heavy on the development of more powerful laser beams.

The other two approaches use strong magnetic fields to contain the fuel, stellarators and tokamaks. The most developed containing facility is the tokamak, a doughnut shaped chamber where the nuclei are contained with a strong magnetic field. This concept has shown its potential in several experiments and much research is put into optimizing it. The nuclei are in a state called plasma in the tokamak. Plasma is a hot ionized gas containing charged and neutral particles that is quasi-neutral and shows collective behavior.

Figure (1.2) shows that the particles need to have a high temperature to achieve fusion. In a future fusion power plant the majority of the heating will come from the fusion process itself. However, the particles need to be initially heated for the fusion process to start. There are a number of methods available for heating the plasma in a future power plant and these have been successfully tested in current experiments. The plasma in a tokamak is heated ohmically by the current, at higher temperature the efficiency of the ohmic heating is lowered as the resistivity gets small. Other heating schemes are needed such as the Neutral Beam Injection (NBI) where highly energetic beams of neutrals are injected into the plasma. NBI functions both as an energy and particle source. Radio frequency waves heat the plasma by interactions through resonances with the particles.

Here we will focus on magnetic confined plasma in a toroidal geometry, specifically in a tokamak. The outline of this kappa is as follows. In chapter (2) we will describe the plasma in four different ways. First we will discuss the single particle motion in a plasma, secondly the kinetic description of the plasma, thirdly the two-fluid approach and finally one-fluid approach or magnetohydrodynamics (MHD) as it is called. We will also discuss the method of taking the gyroaverage for particles in a magnetically confined plasma and two models which take advantage of this, gyrokinetics and gyrofluids. In chapter (3) we will discuss turbulent transport in more detail and its implication for the efficiency for a fusion power plant. Finally in chapter (4) we will give a brief summary of the appended papers.

# CHAPTER 2

# THEORETICAL DESCRIPTIONS OF PLASMAS

In this section we will describe the plasma in four different ways, representing for different levels of approximation. The simplest is the single particle description in which all particles are treated separately and this will give an intuitively feeling for some of the phenomena in the plasma. In this approximation the electromagnetic fields are prescribed and does not change depending on the movements of the particles. In principle the evolution of a closed system of charged particles can be determined by calculating the electromagnetic forces acting upon them from each other and external forces (from a magnetic field). However, even though a fusion plasma is about $10^5$ times less dense than air the number of particles per cubic meter is about $10^{19}$. The interactions between all of these particles is a computational nightmare. Hence the need for models that treat the particles in broader terms, which is why we introduce the three main models of plasma dynamics, the Vlasov theory (or kinetic theory), two-fluid theory and magnetohydrodynamics (MHD). In all of these models the electromagnetic fields are calculated self-consistently with Maxwell's equations. The Vlasov model is the most detailed of the models and follows the evolution of the electron and ion velocity distribution functions. The two fluid model (or multifluid) is the intermediate of the three and describe the plasma as two interacting fluids. The MHD model is the least detailed which approximates the plasma as a single fluid. All of these models have different benefits and drawbacks which we will discuss.

## 2.1 Single particle movement

It is advantageous to discuss the motion of a single particle in the plasma to get an understanding of some of the phenomena that occurs in a plasma. Magnetic confinement relies on a strong magnetic field which creates a Lorentz force.

$$\boldsymbol{F}_L = Ze(\boldsymbol{E} + \boldsymbol{v} \times \boldsymbol{B}) \tag{2.1}$$

Here $\boldsymbol{F}_L$ is the Lorentz force acting upon a particle, Ze is the charge of the particle, $\boldsymbol{E}$ is the electric field, $\boldsymbol{v}$ is the particles velocity and $\boldsymbol{B}$ is the magnetic field.

As a first step we study the case with a stationary, homogeneous magnetic field and the absence of an electric field. In this case the velocity parallel with the magnetic field is constant as the force only act perpendicular to the field. As a consequence of this the particle will not gain any energy. The equation of motion for the two directions perpendicular to the magnetic field becomes:

$$\ddot{v}_{\perp_1} + \left(\frac{qB}{m}\right)^2 v_{\perp_1} = 0 \tag{2.2}$$

$$\ddot{v}_{\perp_2} + \left(\frac{qB}{m}\right)^2 v_{\perp_2} = 0 \tag{2.3}$$

here the dots denote derivatives with respect of time and $\perp_1$, $\perp_2$ denotes the two orthogonal axis perpendicular to the magnetic field. Eq. (2.2) and Eq. (2.3) describes a harmonic oscillator with the oscillation frequency.

$$\omega_c = \frac{|Ze|B}{m} \tag{2.4}$$

This cyclotron frequencies (every particle has its own), and describe one of the fastest phenomena in the plasma. As a result of this it is common to average out the gyromotion to simplify the equations as we will describe later. The particles motion becomes a helix around the magnetic field. The radius of this motion is called the Larmor radius.

$$r_L = \frac{v_\perp}{\omega_c} \tag{2.5}$$

As the cyclotron frequencies are extremely large the Larmor radius are small compared to the size a modern tokamak experiment. This means that the particles are "bound" to the magnetic field lines, greatly limiting the the transport perpendicular to the magnetic field lines.

As a second step we introduce a general constant force $\boldsymbol{F}$. If a part of the force is parallel to the magnetic field the particle will accelerate forever, this will of course not happen in a real plasma as there are other mechanisms to stop that. If the force has a component perpendicular to the magnetic field this will give rise to a drift velocity

$$\boldsymbol{v}_d = \frac{\boldsymbol{F}_\perp \times \boldsymbol{B}}{ZeB^2} \tag{2.6}$$

This velocity will drift the particle from a given magnetic field line.

The discussion above has been done with a straight, infinite magnetic field. However, these type of magnetic fields does not exist in reality. Before introducing more realistic magnetic fields we first need to introduce the concepts of guidingcenter and gyroaveraging. As we have seen, a charged particle gyrates around a magnetic field line, the center of this motion is called the guidingcenter. The gyromotion is

extremely fast, the cyclotron frequency $\omega_c$ is usually much faster than all other relevant plasma phenomena. Hence, we can average over the gyromotion and consider the motion of the guiding center instead of the actual position of the particle. The main benefit of this is that in gyrokinetic modeling it reduces the dimensionality of the problem, thus saving a lot of computational power. The position of the particle can be split up to a gyrocenter part an a fast moving gyration part.

$$\boldsymbol{x} = \boldsymbol{x}_{gc} + \boldsymbol{x}_L, \boldsymbol{v} = \boldsymbol{v}_{gc} + \boldsymbol{v}_L \tag{2.7}$$

here we have $\boldsymbol{v}_{gc}$ as the velocity of the guiding-center which the particle gyrates around. $\boldsymbol{v}_L$ is the velocity of the gyration. The gyroaverage is defined as

$$\langle f \rangle_{\boldsymbol{x}_{gc}} = \frac{1}{2\pi} \oint f(\boldsymbol{x}_{gc}, v_\parallel, v_\perp, \gamma) d\gamma \tag{2.8}$$

here $\gamma$ is the gyroangle. $\boldsymbol{x}_{gc}, v_\parallel$ and $v_\perp$ are kept constant during the averaging. When we have a constant magnetic field, Eq. (2.8) becomes an average over the perpendicular motion. We have $\langle \boldsymbol{x}_L \rangle_{\boldsymbol{x}_{gc}} = 0$, $\langle \boldsymbol{v}_\perp \rangle_{\boldsymbol{x}_{gc}} = 0$ and $\langle \boldsymbol{x} \rangle_{\boldsymbol{x}_{gc}} = \boldsymbol{x}_{gc}$. Here we have the velocity of the guiding-center as $\boldsymbol{v}_{gc} = v_\parallel \hat{\boldsymbol{b}} + \boldsymbol{v}_d$ with the drift velocity from (2.6). Here again we can notice that a straight magnetic field line will not confine the particle if an external force exist due to the drifts.

## 2.2 Slowly varying magnetic field

To this point we have assumed a homogeneous, static magnetic field but we shall now consider a spatial dependence in the magnetic field. This is important for the tokomak as its topology makes it impossible to achieve a constant magnetic field. This is due to the fact that the coils that create the toroidal magnetic field are much closer together on the inside than on the outside of the tokamak. First we are going to look at the case when the magnetic field changes weakly, the characteristic length of the change in the magnetic field must be much bigger than the Larmor radius. We expand the magnetic field around the guiding center:

$$\boldsymbol{B}(\boldsymbol{x}) = \boldsymbol{B}(\boldsymbol{x}_{gc}) + \boldsymbol{x}_L \cdot \nabla \boldsymbol{B}(\boldsymbol{x}_{gc}) + \mathcal{O}(r_L^2) \tag{2.9}$$

her again we have $\boldsymbol{x} = \boldsymbol{x}_{gc} + \boldsymbol{x}_L$. The second term in the equation is much smaller if the magnetic field changes slowly compared to the Larmor radius. This can be seen by taking the ratio of the two terms and denote the characteristic change of the magnetic field as L, then $\nabla \sim 1/L$, hence

$$\frac{|\boldsymbol{x}_L \cdot \nabla \boldsymbol{B}(\boldsymbol{x}_{gc})|}{|\boldsymbol{B}(\boldsymbol{x}_{gc})|} \sim \frac{r_L}{L} \ll 1 \tag{2.10}$$

This holds in a representative fusion reactor. The effective force from the first order change in the magnetic field can be written as:

$$\boldsymbol{F}_{eff} = \langle Ze\boldsymbol{v} \times (\boldsymbol{x}_L \cdot \nabla \boldsymbol{B}(\boldsymbol{x}_{gc})) \rangle_{\boldsymbol{x}_{gc}} \tag{2.11}$$

if we calculate the integral in Eq. (2.8) we end up with:

$$\boldsymbol{F}_{eff} = -mv_{\parallel}^2\boldsymbol{\kappa} - \mu\nabla B \tag{2.12}$$

here $\boldsymbol{\kappa} = \hat{\boldsymbol{b}} \cdot \nabla\hat{\boldsymbol{b}}$ is the magnetic curvature and $\mu = mv_{\perp}^2/(2B)$ is the magnetic moment. These two effective forces have both physical representation. The first term, is a centrifugal force caused by the curvature in the magnetic field. The second term represent the fact that the particle feels a slightly different magnetic field during its gyrating. The weak field side will have a larger Larmor radius than the high field side according to (2.5) and therefore the guiding center will drift.

The magnetic moment is an adiabatic invariant and as such it can be interpreted as a property of the guiding center. The kinetic energy of a particle can be written as $mv_{\parallel}^2/2 + \mu B$, thus we can look at the last term as an effective potential, U. This potential will give rise to a force when the particle crosses from higher or lower magnetic field, $\boldsymbol{F} = -\nabla U$, which represent the second term in Eq. (2.12). This term is called the mirror force as it reflects particles with insufficient kinetic energy to overcome the potential of a stronger magnetic field.

From Eq. (2.6) we can calculate an associated drift velocity from the effective force. If we also let the electric field to be non-zero, $\boldsymbol{E} \neq 0$, with the assumption that the electric field is close to constant over one particle gyration. The velocity for the guiding center becomes

$$\boldsymbol{v}_{gc} = v_{\parallel}\hat{\boldsymbol{b}} + \boldsymbol{v}_d \tag{2.13}$$

where the parallel velocity $v_{\parallel}$ is computed from the parallel component of the force $\boldsymbol{F} = Ze\boldsymbol{E} + \boldsymbol{F}_{eff}$. We get the drift velocity from (2.6)

$$\boldsymbol{v}_d = \frac{\boldsymbol{E}\times\boldsymbol{B}}{B^2} + \frac{v_{\perp}^2}{2\omega_c}\hat{\boldsymbol{b}}\times\nabla logB + \frac{v_{\parallel}^2}{\omega_c}\hat{\boldsymbol{b}}\times\boldsymbol{\kappa} \tag{2.14}$$

where the first term is the so called ExB-drift , the second term is associated with the change in the magnetic field and the third is the curvature-drift. The second term is small due to the ratio $r_L/L$, there again L is the characteristic length of the change in the magnetic field. An interesting thing to notice is that for the two magnetic drifts, there is a charge dependence, hence the ions and electrons will drift in opposite directions. For the ExB-drift however we have no dependence of the charge, thus ions and electrons will drift in the same direction and at the same speed as it is independent of mass.

The drift is small compared to the parallel motion of the particles along the magnetic field, however for the confinement these drifts are important. In the next section we will look how these different drifts affect different magnetic confinements.

### 2.2.1 Chronology of different magnetically confined plasmas

The first historical attempts to confine the particles was in a so called open system, where the magnetic fields lines hit a wall. These machines where long tubes which used the mirror force to confine the particles. The field lines are straight along the tube and at each end where the magnetic field gets stronger, the field lines get closer. If the particle does not have enough parallel velocity it will turn back. These types

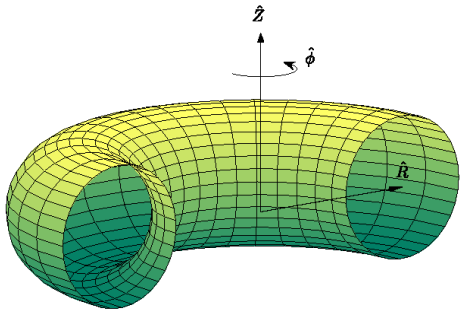


**Figure 2.1:** *Toroidal geometry and coordinates*

of machines have a large loss which cannot be avoided and therefore a new type of machine was invented. This newer device had the magnetic fields never touch a surface which is why they were called closed system. The principle is that the particles will be confined to their field lines. For such system to exist it has been proven that it needs to be topologically a torus [21].

To discuss a toroidal geometry we first need to present a toroidal coordinate system, as shown in Figure (2.1). The coordinate system (Z,R,$\phi$), where R is the distance from the symmetric center, Z the height from symmetric plane and $\phi$ the azimuthal angle. First we will look at a magnetic field with only a toroidal component, $\boldsymbol{B} = B\hat{\phi}$. This can be created by a current in a long conductor passing through origo in the $\hat{z}$-direction. Amperes law gives the strength of the magnetic field

$$B = \frac{\mu_0 I}{2\pi R}\hat{\phi} \tag{2.15}$$

where I is the current and R is the length to the $\hat{z}$-axis. It is clear that the magnetic field decays with R, $B \sim R^{-1}$. This is the same dependency as a realistic toroidal magnetic field in a tokmak which has its toroidal magnetic field created by external currents in coils wound around the minor radia. We can use the discussion in the previous section to state the effective force on the particles in this magnetic field. The effective force on the guiding center, in this toroidal coordinate system, becomes.

$$\boldsymbol{F}_{eff} = \left(\frac{mv_\parallel^2}{R} + \frac{\mu B}{R}\right)\hat{R} \tag{2.16}$$

with this effective force we get the drift as:

$$\boldsymbol{v}_d = \left(v_\parallel^2 + \frac{v_\perp^2}{2}\right)\frac{m}{ZeBR}\hat{Z} \tag{2.17}$$

If we assume that $v_\parallel \sim v_\perp$, we get

$$\boldsymbol{v}_d \sim \frac{r_L}{R}\left(v_\parallel + \frac{v_\perp}{2}\right)\hat{Z} \tag{2.18}$$

Here we see that the drift will be just a fraction of the velocities as $r_L/R$ is small. To get the drift we need to get an average over the whole toroidal motion.

As the particles are locked to the magnetic field lines, this is trivial in the case with a magnetic field with only a toroidal component. In the zeroth order in $r_L/R$ we do not get a drift and the particles are confined by a purely toroidal magnetic field. However, as in a real tokamak the ratio $r_L/R$ is non zero it is clear that the particles will drift from their magnetic field in the $\hat{Z}$-direction.

In order to solve this problem a poloidal magnetic field needs to be added and how you add it is the difference between between tokamaks and stellarators. The tokamaks solution to this is to create a current in the plasma that adds the polidial magnetic field. The stellarators solution is to design the coils in such a way to create a polidial and toroidal magnetic field. The current in the tokamak is created by a large transformer at the center of the machine. The transformer creates one of the limitations on how long an experiment in a tokamak can run as its core gets saturated. One of the advantages with stellarators is that it does not have this limitation. Both these solutions creates a helix magnetic field around the toroidal surfaces. These surfaces are known as flux-surfaces. As these flux-surfaces by no means need to be (or are) circular we need to define a new type of coordinate system. A new radial coordinate, the flux surface label $\rho_t$ which defines a flux-surface, i.e. is constant on them and varies between different flux-surfaces. The flux-label can be defined by the poloidal or the toroidal magnetic flux, in this thesis we will define it as dependent on the toroidal magnetic flux, as denoted by the "t" in $\rho_t$. The normalized $\rho_t$ is defined as:

$$\rho_t = \sqrt{\frac{\Phi - \Phi_{ax}}{\Phi_{sep} - \Phi_{ax}}} \tag{2.19}$$

Here $\Phi$, $\Phi_{ax}$, $\Phi_{sep}$ is the toroidal magnetic flux, the toroidal magnetic flux at the magnetic axis and at the separatrix, respectively. They are defined by:

$$\Phi = \int_{S_t} \boldsymbol{B} \cdot d\boldsymbol{S}_t \tag{2.20}$$

To determine the cumulative results of the drift for these helical magnetic fields is more difficult compared to the purely toroidal fields. We have to study the drift over the time of several laps around the toroidal orbits. For these drifts to cancel each other out we need to look at the average drift over the particle path as it move on the helixial flux-surface until it ends up at its initial position. We describe this path as the length l. If the particle is going to be confined we need to have no net drift in the radial direction, i.e. $\rho_t$. This can be expressed with the integral.

$$\int \boldsymbol{v}_d \cdot \boldsymbol{\nabla} \rho_t dl = 0 \tag{2.21}$$

For this equation to be true the magnetic field strength can not be constant along the field lines, i.e. $\nabla B \cdot dl \neq 0$, as this would, as shown above lead to a drift constant in the same direction. This inequality is achieved as the helical magnetic field lines moves across the major radius, the toroidal magnetic field strength changes, as seen in Eq. (2.15).

As the magnetic field strength varies across the major radius the particles will feel a stronger magnetic force as they move closer to the center of the torus. As

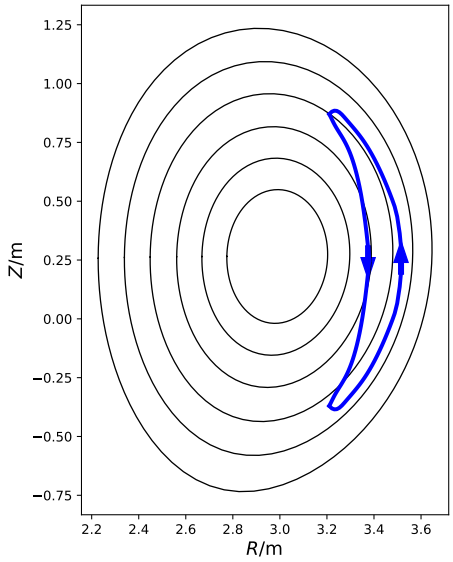


**Figure 2.2:** *The blue line depicts trapped electrons in a "banana"-orbit*

previously discussed this means that some particles with insufficient parallel velocity will turn back. This can be described as $mv_{\parallel}^2 < \mu B_{max}$, there $B_{max}$ is the maximum field strength along the magnetic field line. This magnetic mirror force creates two distinct types of particles, the ones with sufficient parallel velocity, $mv_{\parallel}^2 > \mu B_{max}$ which will make the full orbit along the field line, passing particles. The other type of particles are the ones with too low parallel velocity, these will not make a full orbit and will bounce back and forth, therefore they are called trapped particles. Their orbits are displayed in Figure (2.2) and they are located on the low field side of the tokamak. These particles give rise to an instability called the Trapped Electron Mode (TEM).

## 2.3 Kinetic description

The kinetic description of plasmas is a statistical description of a system of identical particles. We introduce the distribution function, $f(\boldsymbol{x}, \boldsymbol{v}, t)$ which describes the probability to find a particle with velocity $\boldsymbol{v}$ and position $\boldsymbol{x}$ at time t in phase space. The distribution function is closely linked to observable quantities of the plasma, by integrating the distribution function over the velocity we get the particle density,

$$n(\boldsymbol{x}, t) = \int f(\boldsymbol{x}, \boldsymbol{v}, t) d^3v \tag{2.22}$$

This procedure is called taking velocity moments (or only moments) of the distribution function. Eq. (2.22) is the zeroth moment, we multiply the distribution function with $\boldsymbol{v}^0$ and perform integrating. Other macroscopic quantities can be

calculated by taking higher order moments:

$$\textit{Mean velocity} = \boldsymbol{u}(\boldsymbol{x},t) = \frac{1}{n}\int \boldsymbol{v} f(\boldsymbol{x},\boldsymbol{v},t)d^3v \tag{2.23a}$$

$$\textit{Pressure tensor} = \overleftrightarrow{\boldsymbol{P}}(\boldsymbol{x},t) = m\int \boldsymbol{v}'\boldsymbol{v}' f(\boldsymbol{x},\boldsymbol{v},t)d^3v \tag{2.23b}$$

$$\textit{Heat flux vector} = \boldsymbol{Q}(\boldsymbol{x},t) = \int \frac{mv'^2}{2}\boldsymbol{v}' f(\boldsymbol{x},\boldsymbol{v},t)d^3v \tag{2.23c}$$

We have decomposed the velocity: $\boldsymbol{v} = \boldsymbol{u}(\boldsymbol{x},t) + \boldsymbol{v}'(\boldsymbol{x},t)$, here $\boldsymbol{v}'(\boldsymbol{x},t)$ is the random part of a given velocity, hence $\int \boldsymbol{v}' f d^3v = 0$. We now have the connection between the distribution function and measurable quantities, we will now proceed to create a framework to determine the distribution function. To do this we will treat the macroscopic forces (such as the Lorentz force from the electromagnetic fields) and microscopic forces such as the collisional forces. By assuming that the change of particles in a volume in phase-space is equal to the flux in (or out), which means we do not have any sources or sinks in the box (ignoring fusion processes for now). This can mathematically be described as

$$\frac{\partial f}{\partial t} + \boldsymbol{v}\cdot\frac{\partial f}{\partial \boldsymbol{x}} + \boldsymbol{a}\cdot\frac{\partial f}{\partial \boldsymbol{v}} = 0 \tag{2.24}$$

which is the Vlasov equation and is the basis for many of the models in plasma physics. The acceleration comes from the Lorentz force $\boldsymbol{a} = \frac{Ze}{m}(\boldsymbol{E} + \boldsymbol{v}\times\boldsymbol{B})$. This force is determined by the Maxwell's equations:

$$\nabla\cdot\boldsymbol{E} = 4\pi\sum_\sigma Z_\sigma e\int f_\sigma d^3v \tag{2.25a}$$

$$\nabla\cdot\boldsymbol{B} = 0 \tag{2.25b}$$

$$\nabla\times\boldsymbol{E} = -\frac{1}{c}\frac{\partial \boldsymbol{B}}{\partial t} \tag{2.25c}$$

$$\nabla\times\boldsymbol{B} = \frac{4\pi}{c}\sum_\sigma Z_\sigma e\int \boldsymbol{v} f_\sigma d^3v + \frac{1}{c}\frac{\partial \boldsymbol{E}}{\partial t} \tag{2.25d}$$

Here we added $\sigma$ to identify each particle species. Eq. (2.24) does not have collisions included why it also called the collisionless Boltzmann equation. Before we add collisions formally to the equation it is beneficial to discuss how collisions are treated by the kinetic model. This is important as many of these concepts and constraints carries over to the simulations done by the numerical codes. Collisions in plasmas are rare but they have an important role for the dynamics of the plasma. (As a side note we can mention that collisions will be even rarer in future tokamaks as the normalized collisionality goes as $T_e^{-2}$ and future tokamaks are going to be warmer.) A plasma consists of charged particles and as such the collisions originates from electromagnetic effects and not from hard collisions. It is a cumulative effect of small gracing collisions that dominates in the plasma. In the kinetic descriptions a collision is a jump in the velocity coordinate (located at a certain spatial coordinate). If these velocity jumps happen fast enough they can be described such that a particle

at a position in phase space is annihilated and created at another position, as the velocity has changed. The exact details how these jumps occur is not of much interest as it is the cumulative effect which we wish to study. Mathematically these jumps are treated as sinks and sources in phase space and we include them in the Vlasov equation by adding a collision operator on the right hand side of equation, Eq. (2.24).

$$\frac{\partial f_\sigma}{\partial t} + \boldsymbol{v} \cdot \frac{\partial f_\sigma}{\partial \boldsymbol{x}} + \boldsymbol{a} \cdot \frac{\partial f_\sigma}{\partial \boldsymbol{v}} = \sum_\alpha C_{\sigma\alpha}(f_\sigma) \tag{2.26}$$

This is the collisional kinetic equation, called the Boltzmann equation. Here $C_{\sigma\alpha}$ is the rate of change for $f_\sigma$ due to collisions between species $\sigma$ and $\alpha$. The collision operator has number of constraints to conserve a couple of physical quantities.

- Conservation of particles

$$\int C_{\sigma\alpha}(f_\sigma) d^3v = 0 \tag{2.27}$$

- Conservation of momentum

$$\int m_\sigma \boldsymbol{v} C_{\sigma\sigma}(f_\sigma) d^3v = 0 \tag{2.28a}$$

$$\int m_\sigma \boldsymbol{v} C_{\sigma\alpha}(f_\sigma) d^3v + \int m_\alpha \boldsymbol{v} C_{\alpha\sigma}(f_\alpha) d^3v = 0 \tag{2.28b}$$

- Conservation of energy

$$\int m_\sigma v^2 C_{\sigma\sigma}(f_\sigma) d^3v = 0 \tag{2.29a}$$

$$\int m_\sigma v^2 C_{\sigma\alpha}(f_\sigma) d^3v + \int m_\alpha v^2 C_{\alpha\sigma}(f_\alpha) d^3v = 0 \tag{2.29b}$$

## 2.4 Two fluid-models

The kinetic description of the plasma can be somewhat hard to use and is computationally heavy. A different approach to study the plasma is to look at it as a composite of fluids (instead of a group of discrete particles). This can be done by taking moments of the Boltzmann equation, Eq. (2.26) which will create a set of partial differential equations which will couple the mean quantities, presented in Eq. (2.22) and (2.23a), such as $n(\boldsymbol{x}, t), \boldsymbol{u}(\boldsymbol{x}, t)$ etc. If we take the first moment of the Boltzmann equation by multiplying by unity and integrating over the velocity room.

$$\int \left( \frac{\partial f_\sigma}{\partial t} + \boldsymbol{v} \cdot \frac{\partial f_\sigma}{\partial \boldsymbol{x}} + \boldsymbol{a} \cdot \frac{\partial f_\sigma}{\partial \boldsymbol{v}} \right) d^3v = \sum_\alpha \int C_{\sigma\alpha}(f_\sigma) d^3v \tag{2.30}$$

For the two terms on the left hand side the integral commutes with the time and space derivatives as $\boldsymbol{x}, \boldsymbol{v}$ and t is independent variables. We can rewrite the third term so we get $\int \frac{\partial f_\sigma}{\partial \boldsymbol{v}} \cdot (\boldsymbol{a} f_\sigma) d^3v$. This is the volume integral of a divergence in velocity space, hence we can use Gauss theorem to rewrite it: $\oint \boldsymbol{a} f_\sigma \cdot d\boldsymbol{S}$. It is easy to understand that his term will vanish, $f_\sigma \to 0$ as $|v| \to \infty$. This is stating

the fact that the probability to find a particle with infinite velocity is zero. The right hand side is equal to zero as collisions can not change the number of particles. Using this we get:

$$\frac{\partial n_\sigma}{\partial t} + \nabla \cdot (n_\sigma \boldsymbol{u}_\sigma) = 0 \tag{2.31}$$

This is the continuity equation, which is the first equation that constitutes the basis for the two fluid-model. Let us take the first moment of the Boltzmann equation by multiplying it with $\boldsymbol{v}$ and integrating over the velocity:

$$\int \boldsymbol{v} \left( \frac{\partial f_\sigma}{\partial t} + \boldsymbol{v} \cdot \frac{\partial f_\sigma}{\partial \boldsymbol{x}} + \boldsymbol{a} \cdot \frac{\partial f_\sigma}{\partial \boldsymbol{v}} \right) d^3v = \sum_\alpha \int \boldsymbol{v} C_{\sigma\alpha}(f_\sigma) d^3v \tag{2.32}$$

We may rewrite this by using the following

1. Again use the fact the integral commutes with both the time a space derivative for the two first terms on the left hand side
2. Write the velocity as $\boldsymbol{v} = \boldsymbol{u}(\boldsymbol{x}, t) + \boldsymbol{v}'(\boldsymbol{x}, t)$, here $\boldsymbol{v}'(\boldsymbol{x}, t)$ is the random part of a given velocity, hence $\int \boldsymbol{v}' f_\sigma d^3v = 0$.
3. When integrating the third term on the left hand side use the fact that

$$\left( \frac{\partial \boldsymbol{v}}{\partial \boldsymbol{v}} \right)_{ij} = \delta_{ij} \tag{2.33}$$

Here $\delta_{ij}$ is the dirac-delta. By using this we can rewrite (2.32).

$$\frac{\partial (n_\sigma \boldsymbol{u}_\sigma)}{\partial t} + \frac{\partial}{\partial \boldsymbol{x}} \cdot \int (\boldsymbol{v}'\boldsymbol{v}' + \boldsymbol{v}'\boldsymbol{u}_\sigma + \boldsymbol{u}_\sigma \boldsymbol{v}' + \boldsymbol{u}_\sigma \boldsymbol{u}_\sigma) f_\sigma d^3v - \int \boldsymbol{a} f_\sigma d^3v = \sum_\alpha \boldsymbol{R}_{\sigma\alpha} \tag{2.34}$$

The two terms with a single mean velocity $\boldsymbol{u}_\sigma$ in the first integral disappears as $\int \boldsymbol{v}' f_\sigma d^3v = 0$ and $\boldsymbol{u}_\sigma$ is independent of v. We can also see that the first term in the first integral is the pressure tensor, defined in Eq. (2.23b).

Sometimes people do the assumption that $f_\sigma$ is an isotropic function in v as this simplifies the pressure tensor greatly. However this is done purely for mathematical convenience and for real distribution functions isotropy is far from guaranteed. Collisions in the system drives the distribution function towards isotropy but a a sparse hot plasma usually does not have enough collisions. We are going to leave the pressure tensor by its definition from Eq. (2.23b). The right hand side of Eq. (2.34), $\boldsymbol{R}_{\sigma\alpha}$ is the net frictional drag force of species $\sigma$ due to collision with species $\alpha$. As a species can not exert a net force upon itself, $\boldsymbol{R}_{\sigma\sigma} = 0$. Due to the conservation of momentum it follows that $\boldsymbol{R}_{\alpha\sigma} + \boldsymbol{R}_{\sigma\alpha} = 0$.

If we put this all together and assume the only acceleration is created by the Lorentz Force we get the so called momentum equation:

$$n_\sigma m_\sigma \frac{d\boldsymbol{u}_\sigma}{dt} = n_\sigma Z_\sigma e(\boldsymbol{E} + \boldsymbol{u}_\sigma \times \boldsymbol{B}) - \nabla \cdot \overleftrightarrow{\boldsymbol{P}}_\sigma + \sum_\alpha \boldsymbol{R}_{\sigma\alpha} \tag{2.35}$$

Here we used the operator d/dt which is defined as the convective derivative

$$\frac{d}{dt} = \frac{\partial}{\partial t} + \boldsymbol{u}_\sigma \cdot \nabla \tag{2.36}$$

which describes the rate of change seen by an observer moving with the mean fluid velocity $\boldsymbol{u}_\sigma$.

We will now briefly look at the second moment of the Boltzmann equation. This is done by multiplying the Boltzmann equation, Eq. (2.26), with $m_\sigma v^2/2$

$$\int \frac{m_\sigma v^2}{2} \left( \frac{\partial f_\sigma}{\partial t} + \boldsymbol{v} \cdot \frac{\partial f_\sigma}{\partial \boldsymbol{x}} + \boldsymbol{a} \cdot \frac{\partial f_\sigma}{\partial \boldsymbol{v}} \right) d^3v = \sum_\alpha \int \frac{m_\sigma v^2}{2} C_{\sigma\alpha}(f_\sigma) d^3v \tag{2.37}$$

This is the starting point for the derivation of the energy conservation equation, (a derivation can be seen in [1] among others)

$$\frac{3}{2}\frac{dP_\sigma}{dt} + \frac{5}{2} P_\sigma \nabla \cdot \boldsymbol{u}_\sigma = -\nabla \cdot \boldsymbol{Q}_\sigma + \sum_\alpha \left[ \boldsymbol{R}_{\sigma\alpha} \cdot \boldsymbol{u}_\sigma - \left( \frac{\partial W}{\partial t} \right)_{E\sigma\alpha} \right] \tag{2.38}$$

The last term on the right hand side is the rate which the species $\alpha$ collisionialy transfers to species $\sigma$ and is defined as:

$$\left( \frac{\partial W}{\partial t} \right)_{E\sigma\alpha} = -\sum_\alpha \int \frac{m_\sigma v^2}{2} C_{\sigma\alpha}(f_\sigma) d^3v \tag{2.39}$$

We also have the heat flux defined in Eq. (2.23a).

The equations (2.31), (2.35), and (2.38) are a set of coupled differential equations. These are called the Braginskii equations [2]. One very important thing to notice about these equations is that a pattern appears. When we took the zeroth moment to derive an equation for the density we got a term with the mean velocity. In the same way when we took the first moment to derive an equation for velocity we got a term with pressure. And finally for the second moment, in the equation for the energy we got a higher order term as well. This is an open system. To create a system of equation which can be solved some closure is needed. This can be done in several ways, some of them are assuming adiabatic or isothermal processes. More advanced closures have been developed which are valid also in the weak collisionality limit relevant to the core region of fusion plasmas. An example is the fluid model developed at Chalmers [25] which has been successfully used to analyze and predict tokamak experiments at JET. The equations (2.31), (2.35), and (2.38) are the fundamental equations for two-fluid models. The aforementioned equations can be easily generalized for more ion species, for example to take into account a second main ion species, as in a Deuterium-Tritium plasma, or impurities.

## 2.5 Magnetohydrodynamics

As the plasma is composed of ions an electrons it is natural to describe the plasma as two fluids. We can however go one step further and describe all particles in the

plasma as one fluid. This model is the simplest we are going to look at and it is called Magnetohydrodynamics (MHD). For this model to be valid the plasma needs to be collision dominated and it include low-frequency, long-wavelength, magnetic behavior of the plasma. MHD has a macroscopic point of view compared to the kinetic theory and the two-fluid model. In the following section we will derive the so called Grad-Shafranov equation which defines the static magnetic geometry with nested flux surfaces. We use flux coordinate system in our transport simulations.

The characteristic properties for the MHD model are, the total mass density $\rho$, the total charge density $\rho_c$, the center of mass velocity $\boldsymbol{U}$ and the current density $\boldsymbol{J}$:

$$\rho \equiv m_i n_i + m_e n_e \tag{2.40a}$$
$$\rho_c \equiv e(Z_i n_i - n_e) \tag{2.40b}$$
$$\boldsymbol{U} \equiv \frac{m_i n_i \boldsymbol{u}_i + m_e n_e \boldsymbol{u}_e}{m_i n_i + m_e n_e} \tag{2.40c}$$
$$\boldsymbol{J} \equiv e(Z_i n_i \boldsymbol{u}_i - n_e \boldsymbol{u}_e) \tag{2.40d}$$

Here $m_i, m_e, n_i, n_e, \boldsymbol{u}_i$ and $\boldsymbol{u}_e$ are the masses, densities and fluid velocities for the ions and electrons. If we use the assumption of quasi neutrality, i.e $Z_i n_i \approx n_e$, we notice that the charge density vanishes.

The derivation of the equations that governs MHD are similar to the one done for the two fluid model in the previous section. This is done by again taking moments of the Boltzmann equation, Eq. (2.26), but now multiplying it with $m_\sigma$ and take the sum over all particle species. The MHD continuity equation is trivially derived.

$$\frac{\partial \rho}{\partial t} + \nabla \cdot (\rho \boldsymbol{U}) = 0 \tag{2.41}$$

This equations states mass conservation. The momentum equation is derived by taking the first moment and take the sum over all species:

$$\frac{\partial}{\partial t} \sum_\sigma m_\sigma \int \boldsymbol{v} f_\sigma d^3v + \frac{\partial}{\partial \boldsymbol{x}} \cdot \Sigma_\sigma \int m_\sigma \boldsymbol{v}\boldsymbol{v} f_\sigma d^3v + \sum_\sigma q_\sigma \int \boldsymbol{v} \frac{\partial}{\partial \boldsymbol{v}} \cdot [(\boldsymbol{E} + \boldsymbol{v} \times \boldsymbol{B}) f_\sigma] = 0 \tag{2.42}$$

Here we have zero on the right hand side as $\boldsymbol{R}_{\sigma\alpha} + \boldsymbol{R}_{\alpha\sigma} = 0$ , the plasma can not add to its own momentum. In MHD we will define the relative velocities compared to the center of mass velocity, $\boldsymbol{v}_\sigma = \boldsymbol{U} + \boldsymbol{v}^*_\sigma$. The integral in the second term can then be written as,

$$\sum_\sigma \int m_\sigma \boldsymbol{v}_\sigma \boldsymbol{v}_\sigma f_\sigma d^3v = \sum_\sigma \int m_\sigma (\boldsymbol{U} + \boldsymbol{v}^*_\sigma)(\boldsymbol{U} + \boldsymbol{v}^*_\sigma) f_\sigma d^3v = \sum_\sigma \int m_\sigma \boldsymbol{v}^*_\sigma \boldsymbol{v}^*_\sigma f_\sigma d^3v + \rho \boldsymbol{U}\boldsymbol{U} \tag{2.43}$$

where the parts with a single $\boldsymbol{v}^*_\sigma$ are discarded as $\sum_\sigma \int m_\sigma \boldsymbol{v}^*_\sigma f_\sigma d^3v = 0$. We define the MHD pressure tensor which is given by the random velocities relative to $\boldsymbol{U}$.

$$\overleftrightarrow{\boldsymbol{P}}^{MHD} = \sum_{\sigma} \int m_{\sigma} \boldsymbol{v}_{\sigma}^{*} \boldsymbol{v}_{\sigma}^{*} f_{\sigma} d^{3}v \tag{2.44}$$

The third term in Eq. (2.42) can be integrated by parts, which we can use to get the following expression:

$$\frac{\rho \boldsymbol{U}}{\partial t} + \nabla \cdot (\rho \boldsymbol{U}\boldsymbol{U}) = \left( \sum_{\sigma} n_{\sigma} q_{\sigma} \right) \boldsymbol{E} + \boldsymbol{J} \times \boldsymbol{B} - \nabla \overleftrightarrow{\boldsymbol{P}}^{MHD} \tag{2.45}$$

Here we can use the quasi neutrality criteria and see that the term with the electric field vanishes. The two first terms can be expanded:

$$\begin{aligned} \frac{\rho \boldsymbol{U}}{\partial t} + \nabla \cdot (\rho \boldsymbol{U}\boldsymbol{U}) &= \underbrace{\left( \frac{\partial \rho}{\partial t} + \nabla \cdot (\rho \boldsymbol{U}) \right)}_{\text{continuity equation}} \boldsymbol{U} + \rho \frac{\partial \boldsymbol{U}}{\partial t} + \rho \boldsymbol{U} \cdot \nabla \boldsymbol{U} \\ &= \rho \left( \frac{\partial \boldsymbol{U}}{\partial t} + \boldsymbol{U} \cdot \nabla \boldsymbol{U} \right) \end{aligned} \tag{2.46}$$

Now we are ready to write the momentum equation for MHD in its standard from

$$\rho \frac{D\boldsymbol{U}}{Dt} = \boldsymbol{J} \times \boldsymbol{B} - \nabla \cdot \overleftrightarrow{\boldsymbol{P}}^{MHD} \tag{2.47}$$

with

$$\frac{D}{Dt} = \frac{\partial}{\partial t} + \boldsymbol{U} \cdot \nabla \tag{2.48}$$

This is the convective derivative defined by the center-of-mass velocity unlike the separate fluid velocities which we used for the two-fluid model. If we assume an isotropic MHD pressure we can replace the tensor with a scalar pressure, P. The static equilibrium, Eq. (2.47) becomes:

$$\boldsymbol{J} \times \boldsymbol{B} = \nabla P \tag{2.49}$$

This equation describes the equilibrium between the magnetic pressure and tension, described by $\boldsymbol{J} \times \boldsymbol{B}$ and the total particle pressure, $\nabla P$. The solution to this equation in two dimensions (an axi-symmetric cylindrical plasma) gives rise to the so called Bennett pinch or z-pinch. It was found that, theoretically, a small current could contain a considerable plasma pressure. However, these types of devices are highly unstable. Although Eq. (2.49) looks simple the solution in three dimensions is far from it. It can be written as a differential equation for the poloidal flux function $\psi$, and it has two arbitrary functions $p(\psi)$ and $F(\psi)$. The function $p(\psi)$ represent the particle pressure and the function $F(\psi)$ is related to the combined poloidal current flowing in the plasma plus the toroidal field coils. A derivation can be found in [20] among others:

$$R^2\nabla\cdot\left(\frac{\nabla\psi}{R^2}\right) = -\mu_0 R^2\frac{dp}{d\psi} - \frac{1}{2}\frac{dF^2}{d\psi} \tag{2.50}$$

Here R is the major radius and $\mu_0$ the magnetic permeability. From the solution for $\psi$ the radial coordinate $\rho_t$, introduced in Chapter (2.2.1), can be determined. Numerical solutions of the equation describe the flux-surfaces and are used in simulation codes to describe the magnetic equilibrium. There are a number of analytical approximate solutions to the equation, one commonly used is the Miller model. The Miller model is an approximate description of each flux surface with nine parameters. These parameters describe different aspects of the magnetic equilibrium and many of these are crucial to confinement of the plasma. One of the most important is the safety factor q. The plasma current creates a poloidal magnetic field which makes the field line bend around the torus, the sharpness of the bend define the safety factor:

$$q = \frac{n_t}{n_p} = \frac{\langle \boldsymbol{B}\nabla\phi\rangle}{\langle \boldsymbol{B}\nabla\theta\rangle} \tag{2.51}$$

Here $n_t$ is the number of toroidal turns compared to the number of poloidal turns $n_p$. The brackets denote flux surface averaging and the safety factor describes how twisted the magnetic fields are. It is a function of radial position and how rapid it changes is described by the magnetic shear.

$$\hat{s} = \frac{1}{q}\frac{\partial q}{\partial r} \tag{2.52}$$

Other important parameters are the aspect ratio ($\epsilon = r/R$), the elongation ($\kappa$) which describes the difference in length of the axis, triangularity ($\delta$) which describes the shape of the flux-surface etc. An example of the miller description can be seen in Figure (2.3) a) and the major radial dependence of the toroidal magnetic field, pressure and the magnetic current are shown in Figure (2.3) b).

## 2.6 Gyrokinetics

As mentioned in section (2.1), the charged particles are ”bound” to a magnetic flux surface due to the Lorentz force. Hence it is sometimes more prudent to study the evolution of the the so called guiding-centers rather than the particles themselves. This can be taken a further step to the so called gyrocenter, as the guiding center still follows the particle true position, but with the guiding center as a reference. When handling gyrocenter the exact trajectory is of no interest and instead we follow the evolution of ”charged rings”. The quick gyromotion compared to the electromagnetic fluctuations is the basis of the so called gyrokinetic theory. By averaging out the fast gyromotion, the number of dimensions of the problem is reduced by one and a time step much greater than the gyroperiod is feasible. This is a great benefit for computational cost.

The modern derivation of the gyrokinetic theory is done by using phase space coordinate transformations which eventually result in equations of motion

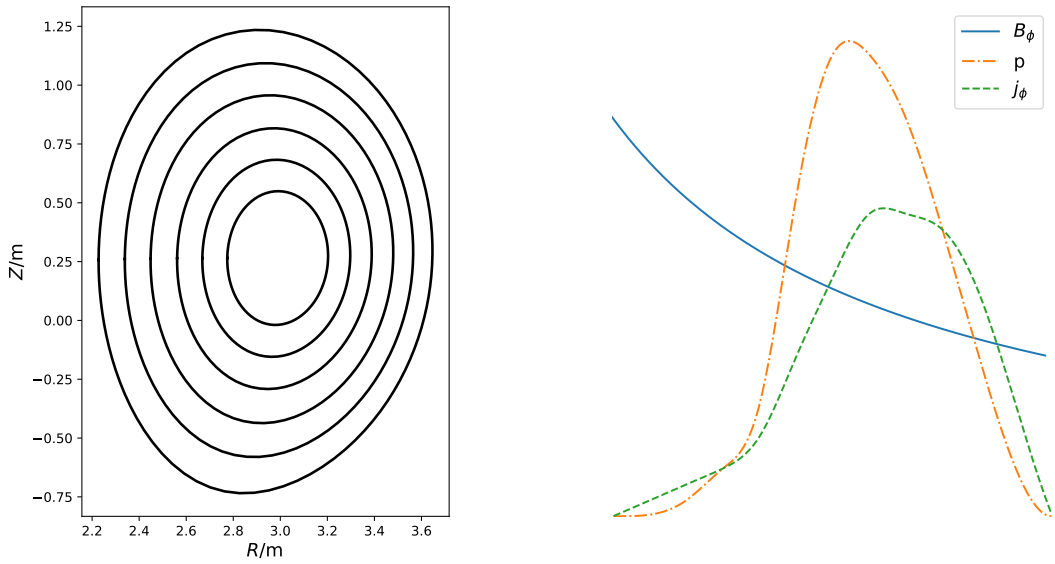


**(a)** Flux-surfaces

**(b)** $B_\phi$, p and $j_\phi$ versus major R

**Figure 2.3:** Miller description of the flux surfaces. The figure to the right show the dependence of the major radial coordinate for the toroidal magnetic feld,$B_\phi$, the toroidal current $j_\phi$, and the plasma pressure, p

that are independent of the gyrophase angle. This derivation uses transformation first to the guiding-center and then to the gyrocenter by using Lie-formalism. A derivation can be found in [3]. Earlier derivations employed perturbation expansions and a direct gyrophase averaging. Both of these methods do however rely on the gyrokinetic ordering. The Larmor radius needs to be small in comparison to the scale length of the change in the background magnetic field, background densities and the background temperatures. The cyclotron frequency need to be much smaller than the frequency of turbulent fluctuations, $\omega/\omega_c \ll 1$. As the particles velocities along the magnetic field line are much greater than the drift velocities perpendicular to the fields, the spatial scales will be very different. The turbulence along the magnetic field lines are "stretched out" compared to the turbulence perpendicular which is comparable with the Larmor radius in scale. We can safely assume:$|\boldsymbol{k}_\parallel|/|\boldsymbol{k}_\perp| \ll 1$. We can summarize the gyrokinetic ordering:

$$\epsilon \sim \frac{\rho_i}{L_B} \sim \frac{\rho_i}{L_B} \sim \frac{\omega}{\omega_c} \sim \frac{e\delta\phi}{T} \sim \frac{|\boldsymbol{k}_\parallel|}{|\boldsymbol{k}_\perp|} \ll 1 \tag{2.53}$$

In gyrokinetic theory we do not study the evolution of the distribution in phase space, f$(\boldsymbol{x}, \boldsymbol{v}, t)$, but instead the study the gyrocenter distribution function in gyrocenter phase space F$(\boldsymbol{X}, v_\parallel, \mu)$. $\boldsymbol{X}$ is the gyrocenter position, $v_\parallel$ is the gyrocenter parallel velocity and $\mu$ is here again the magnetic moment, $\mu = mv_\perp^2/(2B)$. We can rewrite the Vlasov equation, Eq. (2.24), in these coordinates:

$$\frac{\partial F}{\partial t} + \frac{d\boldsymbol{X}}{dt} \cdot \nabla F + \frac{dv_\parallel}{dt}\frac{\partial F}{\partial v_\parallel} + \frac{d\mu}{dt}\frac{\partial F}{\partial \mu} = 0 \tag{2.54}$$

The last term will disappear as the magnetic moment is constant. We decompose the electromagnetic fields into a background and a fluctuating part i.e. $\Phi \to \Phi_0 + \Phi_1$, $\boldsymbol{A} \to \boldsymbol{A}_0 + \boldsymbol{A}_1$. With this we can write the drift velocities for the gyrokinetic theory, here in Gaussian units.

- E x B drift
$$\boldsymbol{v}_\chi = -\frac{c}{B_0^2}\nabla\langle\Phi_1\rangle_{\boldsymbol{x}_{gc}} \times \boldsymbol{B}_0 \tag{2.55}$$
- $\nabla B$-drift
$$\boldsymbol{v}_{\nabla B} = \frac{\mu}{m\omega_c}\hat{b} \times \nabla B_0 \tag{2.56}$$
- curvature drift
$$\boldsymbol{v}_c = \frac{v_\parallel^2}{\omega_c}(\nabla \times \hat{b})_\perp \tag{2.57}$$

Here again $\langle f\rangle_{\boldsymbol{x}_{gc}}$ denotes gyroaveraging. These velocity drifts are the equivalent of the drifts presented in Eq. (2.14). The fluctuating parts need to be much smaller than the background fields. We get the time derivative in these coordinates:

$$\frac{d\boldsymbol{X}}{dt} = v_\parallel\hat{b} + \frac{B_0}{B_{0\parallel}^*}(\boldsymbol{v}_\chi + \boldsymbol{v}_{\nabla B} + \boldsymbol{v}_c) \tag{2.58}$$

$$\frac{dv_\parallel}{dt} = -\left(\frac{\hat{b}}{m} + \frac{B_0}{mv_\parallel B_{0\parallel}^*}(\boldsymbol{v}_\chi + \boldsymbol{v}_{\nabla B} + \boldsymbol{v}_c)\right) \cdot \left(Ze\nabla\langle\Phi_1\rangle_{\boldsymbol{x}_{gc}} + \mu\nabla B_0\right) \tag{2.59}$$

$$\frac{d\mu}{dt} = 0 \tag{2.60}$$

Using all this we can write down the gyrokinetic Vlasov equation, here with $\sigma$ denoting particle species:

$$\begin{aligned}&\frac{\partial F_\sigma}{\partial t} + \left(v_\parallel\hat{b} + \frac{B_0}{B_{0\parallel}^*}(\boldsymbol{v}_\chi + \boldsymbol{v}_{\nabla B} + \boldsymbol{v}_c)\right)\\ &\cdot\left(\nabla F_\sigma + \frac{1}{m_\sigma v_\parallel}\left(-Ze\nabla\langle\Phi_1\rangle_{\boldsymbol{x}_{gc}} - \mu\nabla B_0\right)\frac{\partial F_\sigma}{\partial v_\parallel}\right) = 0\end{aligned} \tag{2.61}$$

With $B_{0\parallel}^* = B_0 + \frac{B_0}{\omega_c}v_\parallel\hat{b}\cdot(\nabla\times\hat{b})$. In order to add collisions, we need to add a collision operator on the right hand side of the equation.

The distribution can be decomposed into a macroscopic part and a part describing the microturbulence with the assumption that the perturbed part is much smaller than the background, $F_\sigma \to F_{\sigma 0} + f_{\sigma 1}$. By using the gyrokinetic ordering to Eq. (2.61) to the zeroth order and decompose the distribution function we can see an interesting thing: The background distribution does not explicitly evolve in time. This is used in $\delta f$-codes to choose a background distribution function which

fulfills the zeroth order. As collisions drives the backgound distrubution towards a Maxwellian distrubution, this is the choice for gyrokinetic codes. GENE is a gyrokinetic code which uses the $\delta f$-approach [22].

In order to solve the gyrokinetic equation a suitable coordinate system needs to be established. Before we embark onto that subject it is important to remind us that the many physical phenomena and structures in a plasma is highly anisotropic. The particles move along the magnetic field lines at high speed but move across them (due the drift velocities among other things) magnitudes slower. Hence the correlation length in the parallel direction is much longer than the perpendicular (this is also one of the assumption we used when introducing the gyrokinetic equation). This knowledge makes it possible to use different resolutions in different spatial coordinates and thus saving a large amount of computational cost. As we have a distinctive direction, which is the magnetic field, a coordinate system aligned to it is a natural construction. A good overview of flux coordinates can be found in [6]. To study the microturbulence for an entire present day tokamak, the required grid-size makes this simulation extremely expensive. These kind of simulations are done today on supercomputers but are rare. In order to systematically study a plasma phenomenona the simulation domain is significantly reduced. This is done with the flux tube approximation. In this approximation a magnetic field is followed around the torus for a poloidal turn (for tokamaks, due to the axisymmetry). A curved and sheared box is created around this magnetic field. The magnetic geometry of this box is not calculated self-consistently with the turbulent fluctuations but is a numerical or an analytical solution to the Grad-Shafranov equation, Eq. (2.50). This box is of a small size compared to the size of the tokamak and the investigation of the plasma is therefore a local one for the flux tube approximation. Because it is a local investigation background quantities such as density and temperature as well as their radial gradients are kept constant throughout the box. This approximation is valid if the radial size of the box is small compared to the machine size but large enough compared to the microturbulence. The coordinate are x for the fluxlabel, i.e. the radial direction which is perpendicular to the flux surface, y is the binormal direction and z is the direction along the field line. As the flux tube approximation only covers a small part of the plasma we need to adapt proper boundary conditions which do not interfere with the physical phenomena which we want to study. In the radial and binormal coordinate periodic boundary conditions are a good choice.

$$F(x + L_x, y, z) = F(x, y, z) \ , \ F(x, y + L_y, z) = F(x, y, z) \tag{2.62}$$

Here $L_x$ is the box size in the x direction and $L_y$ is the box size in the y-direction. These boundary conditions also keep the number of particles and the energy conserved in the x and y direction. This ensure no accumulation of particles inside the simulation box. These periodic boundary conditions also ensure that we can make a Fourier representation in the two perpendicular directions. As the microinstabilities usually are localised at the bad curvature side (the low field side), the flux tube are joined at the high field (inner) side. For the case with a tokamak we only need to do one turn, we get constraints in the metric components due to the joining. This leads to a constraint on the distribution function, here with Fourier

representation for the perpendicular directions. In the direction of the field line:

$$F(k_x, k_y, \pi) = (-1)^{nN} F\left((m + nN)\frac{2\pi}{L_x}, k_y, -\pi\right) \tag{2.63}$$

with $m = k_x \frac{L_x}{2\pi}, n = k_y \frac{L_y}{2\pi}$, for more detail see [24].

## 2.7 Gyrofluid

In the same manner as we got the fluid equations from the Boltzmann equation by taking moments we can get the gyrofluid equations from taking moments of the gyrokinetic equation, Eq. (2.61). The gyrofluid equations are equivalents to the fluid equations, Eq. (2.31), (2.35), and (2.38) and describe the evolution of the plasma. Thanks to the manner the gyrokinetic equation is derived, with the gyroaveraging, the gyrofluid approach has a number of gyroeffects that is not presence in fluid description of the plasma. Finite Larmor Radius (FLR) effects to all orders are naturally included in the gyrofluid equations, in the fluid models only first order FLR effects are usually included and higher order effects have been known to be added manually. FLR effects takes into account the average of fields over the fast gyration of a charged particle around the magnetic field that appears due to the small but non-zero size of the Larmor radius. Another phenomena is Landau damping which is included in the gyrofluid description through the closure used. Landau damping is the mechanism where a wave in the plasma lose (or gain) energy from interacting with particles. If the distribution function is monotonically decreasing with velocity, the plasma gains energy from the wave thereby damping the wave. For a description of taking velocity moments of the gyrokinetic equations see [19], among others.

# CHAPTER 3

# TURBULENT TRANSPORT

In order to make fusion an economically viable energy source, the fusion triple product, $n\tau_E T$, must be maximized. $n$ is the particle density, $\tau_E$ is the energy confinement time and T is the temperature. The product was first introduced by John D. Lawson [23] and is used to describe a lower limit for ignition of the plasma. An ignited plasma is self-sustained from energy from the fusion reactions. To maximize the product there are unfortunately limitations for the density and temperature. The density is limited by the Greenwald limit, which is an empirical stability condition and relates the averaged density to the Plasma current: $\bar{n}/10^{20} = \kappa J$, where $\kappa$ is the elongation and J is the plasma current in $MA/m^3$ [26]. The temperature (and density) are limited by the constrains on $\beta = \frac{nT}{B^2/2\mu_0}$ which describes the fraction between the plasma pressure and the magnetic pressure. If this fraction becomes to large, certain MHD instabilities will occur and disrupt the plasma. This limitation of the $\beta$ is described by the Troyon Limit which includes the conditions for the so called ballooning and the kink mode. These limits can be relaxed by creating a higher plasma current and a stronger magnetic field. This is however a challenging engineering problem. Hence, to improve the confinement time for the plasma is an interesting avenue to optimize the fusion triple product. At the lowest level, the diffusion (and confinement) in a plasma is determined by Coulomb collisions, which describes classical diffusion. Additions to this model were made in the 1960's when Galeev and Sagdev developed the so called neo-classical theory. This new theory incorporated the effects of the particle drifts from the non-uniform magnetic field which is inevitably in a torus shape. This theory suggested that the transport perpendicular to the flux surfaces were small and made plasma physicists hopeful that in a matter of decades that fusion power would be on the electric grid. Alas, this was not to be as we well know. The neo-classical theory is successful at describing the transport along field lines, however perpendicular to the flux surface it is magnitudes away from experimental values. This new, unexpected transport was named anomalous transport to display its unfortunately surprising nature. Today we know that the anomalous transport is caused by microturbulence in the plasma. Small fluctuations of the densities, temperatures, electrostatic potential etc. in the plasma will normally lead to turbulent transport. The study of the turbulent transport is

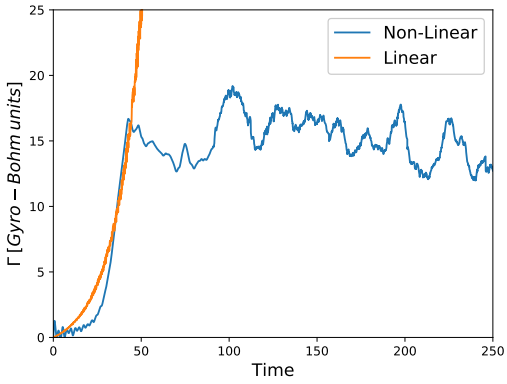


**Figure 3.1:** *The linear and non-linear phase of a gyrokinetic simulation of the DIII-D discharge 165303*

the main goal of this thesis.

## 3.1 Linear, Quasi-Linear and Non-Linear modelling

The models which we have described in chapter (2), the fluid and kinetic models can be used in three distinctive ways: linear, quasi-linear or non-linear. The linear and non-linear simulations are ways to run your model while the quasi-linear model is using results from linear simulations in combination with estimates of the fluctuation levels to estimate measurable quantities such as fluxes. Linear models does not include non-linear terms and are much faster to solve. The easiest way to explain the difference between the two models is by looking at Figure (3.1) where we display the particle flux for a linear and non-linear simulation. The two simulations follow a similar pattern in the initial phase, both grows exponentially and the linear terms are much larger than the non-linear terms. However at a certain level the non-linear terms will become of the same magnitude as the linear terms and couplings between stable and unstable modes become important. This results in a stationary turbulent flux as can be seen in Figure (3.1) for the non-linear simulation.The linear simulation does not include the non-linear terms which creates this coupling, thus grows exponentially forever. In the linear simulations the growthrate and the real frequency are the interesting parts. For the non-linear simulation the particle flux is saturated to a realistic value for the plasma but they are computationally much more expensive than linear simulations.

Quasi-linear theory assume linear relations, even in the non-linear stationary turbulent state, between the fields. The theory describes the connection between the growthrates, real frequencies and other plasma parameters to the saturated particle flux. This have been done both theoretically and ad-hoc by comparing with non-linear simulations. Even though theoretical understanding have helped derive quasi-linear expressions for the fluxes it is often necessary to compare and normalise with non-linear simulations to achieve good comparisons with experiments.

As quasi-linear simulations are computationally much cheaper than non-linear simulations, they are ideal for integrated modeling. The quasi-linear turbulent transport is given by

$$\langle \Gamma_{QL} \rangle = \langle v_{ExB} \delta n \rangle \tag{3.1}$$

here $v_{ExB}$ is the ExB-drift velocity presented in Chapter (2) and $\delta n$ the fluctuating part of the density. These parameters can be calculated numerically or can be expressed analytically to gain a better understanding of the transport. An analytical expression consist of two parts, a linear response (or quasilinear weight) and a quasi-linear intensity. The linear response govern the relation between the fluctuating part of the density, $\delta n$ and the electrostatic potential $\phi$. The quasilinear intensity describes the saturation of the electrostatic potential, which usually consist of a mixing-length assumption. This can be expressed as in [5], here without the mixing length assumption.

$$\begin{aligned}\langle \Gamma_{QL} \rangle =& \Sigma_k \left\langle \frac{k_y c_s^2}{\omega_{ci}} \int F_M \frac{(\hat{\gamma}_k + \hat{\nu}_k)[R/L_{\langle n \rangle} + (E/T_e - 3/2)R/L_{\langle T_e \rangle}] - (\hat{\gamma}_k \hat{\omega}_{Gk} + \hat{\omega}_{rk}\hat{\nu}_k)}{(\hat{\omega}_{rk} + \hat{\omega}_{Gk})^2 + (\hat{\gamma}_k + \hat{\nu}_k)^2} \right. \\ & \left. \times J_0 (k_\perp \rho_s)^2 |\hat{\phi}|_k^2 \right\rangle \end{aligned} \tag{3.2}$$

Where $\gamma$ is the growthrate of the mode and $k_y$ is the associated wave number. $\hat{\nu}_k$ is the collision-frequency, $F_M$ is the equilibrium Maxwellian distribution function and all quantities with a hat in Eq. (3.2) are normalized with the fluid perpendicular drift frequency, $\omega_{Dk} = k_y \rho_s c_s / R$. We have introduced the gradient length: $L_{\langle X_e \rangle} := -\left( \langle |\boldsymbol{\nabla} \rho_t| \rangle \frac{\partial}{\partial \rho_t} \ln \langle X_e \rangle \right)^{-1}$. The brackets denote flux surface averaging. This equation is interesting as it contains a lot of information and dependencies on different plasma parameters. We can first notice that the expression is divided into three specific parts. We have one part which is proportional to the density gradient, this part is the diffusive part and is directed outwards. We have one term proportional to the temperature gradient and is called the thermo-diffusion part. The last part is not dependent on any of the gradients of the density or temperature and is the pinch part which can be directed inwards or outwards. The thermo-diffusion and the pinch can be added together which we will do from here on. From these observations we can define a decomposed particle flux of a diffusive and pinch part, here in a non-circular geometry as we included the metric components $\langle |\boldsymbol{\nabla} \rho_t| \rangle$ and $\langle |\boldsymbol{\nabla} \rho_t|^2 \rangle$. (for details see Paper D)

$$\langle \Gamma_e^{\rho_t} \rangle = -D^{PB}_{\langle n_e \rangle} \langle |\boldsymbol{\nabla} \rho_t|^2 \rangle \partial_{\rho_t} \langle n_e \rangle + V^{PB}_{\langle n_e \rangle} \langle |\boldsymbol{\nabla} \rho_t| \rangle \langle n_e \rangle \tag{3.3}$$

Here $\partial_{\rho_t} = \partial / \partial \rho_t$, $D^{PB}_{\langle n_e \rangle}$ is the diffusion and $V^{PB}_{\langle n_e \rangle}$ is the convective pinch. It is beneficial to discuss the characteristics of the diffusivity and pinch in Eq. (3.3). These transport coefficients are already flux-surface averaged quantities. In addition, the particle balance diffusion does not have an explicit dependency on $\langle n_e \rangle$ i.e. $\partial D^{PB}_{\langle n_e \rangle} / \partial_{\rho_t} \langle n_e \rangle = 0$, and the particle balance pinch does not have an explicit dependency on $\partial_{\rho_t} \langle n_e \rangle$ i.e. $\partial V^{PB}_{\langle n_e \rangle} / \partial \partial_{\rho_t} \langle n_e \rangle = 0$. However, they are dependent on, together with other parameters, the growth rates, which can be seen in Eq. (3.2),

which in their turn are dependent on the density gradient. The way Eq. (3.3) should be viewed is as a decomposition of the flux rather than an equation that shows linear relationships.

## 3.2 Drift modes

Drift waves are an important type of microinstability which occur in the plasma and are associated with the free in the temperature and density gradients. A simple (but informative) ansatz for the transport coefficients is the mixing length estimate which gives the scaling for the effective diffusion:

$$D \sim \frac{\delta x^2}{\delta t} \sim \frac{\gamma}{k_\perp^2} \tag{3.4}$$

Here $\gamma$ is the growth rate of the mode and $k_\perp$ is the associated wavenumber. This relation describes the spatial scale of an instability and determines the total amount of transport. A faster growing mode might not be as important as one with lower growthrate if its spatial scale is much smaller. This is true for the relation between the Ion Temperature Gradient (ITG)-mode and the Electron Temperature Gradient (ETG)-mode. These are equivalent but the ITG-mode is on ion Larmor scale and ETG-mode on electron Larmor radius scale, which means what the ITG-mode is (usually) much more significant. The nature and the origin of these instabilities will be discussed in the following sections.

### 3.2.1 Ion temperature gradient mode

The driftwave which is responsible for most of the turbulent transport in today's plasma experiments is the Ion Temperature Gradient (ITG) - mode. The ITG-mode is a Rayleigh–Taylor type instability where a lighter fluid pushes into a heavier one. The mode is associated with the free energy of the ion temperature gradient and the largest growthrate is of the spatial scale $k_y\rho_i \sim 0.3$. This is much smaller than the tokamak minor radius but large compared with the debye-length. Therefore the quasineutrality condition holds for the perturbed density associated with this mode, $\Sigma_j Z_j e\delta n_j = 0$, which we will use when discussing the origin of mode. The real frequencies of this mode is of the same magnitude as for the diamagnetic drift velocity.

The ITG-mode is formed by a series of physical events which creates a positive feedback loop. A simple way to describe the ITG -mode is to start with a small fluctuation in the ion temperature in the poloidal direction, $\delta T_i$. This leads to a difference in the magnetic drift velocity as it is dependent on the temperature, see Eq. (2.14). The different velocities leads to compression of the ion density in the poloidal direction, $\delta n_i$.

This fluctuation in the ion density is followed by a fluctuation in the electron density as we assume the fluctuations follow quasineutrality. If we assume Boltzmann distributed electrons (and for now ignore trapped electrons):

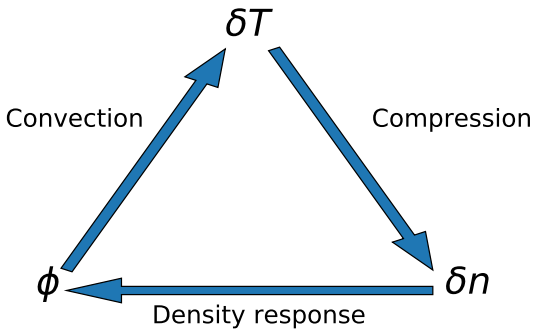


**Figure 3.2:** *Feedback loop for the ITG-mode*

$$\delta n_e = n_e \frac{e\phi}{T_e} \tag{3.5}$$

The fluctuation in the electron density creates an electric field in the poloidal direction. The ExB drift , the first term in Eq. (2.14), is in the radial direction. If the background temperature gradient and magnetic field gradient are in the same direction (low field side), the ExB drift will transport hot particles to hot regions and drive the instability. In the reverse case when the background temperature gradient and magnetic field gradient are in the opposite direction (the high field side) hot particles will get transferred to colder regions, essentially killing the instability. This is why the low field side is called the bad curvature region, which is where the largest fluctuations is encountered on the poloidal plane. This is referred as ballooning. The feedback-loop for the ITG-mode is displayed in Figure (3.2).

As the ITG-mode is such an important instability it has been extensively studied over the years. It has been discovered both analytically and experimentally that there is a cut-off Temperature-gradient [25], [16]. If the temperature gradient is sufficiently low the ITG-mode is stable.

### 3.2.2 Trapped Electron mode

Due to the higher magnetic field at the inner major radius electrons can be trapped at the outer, low field side of the torus. These particles do not travel around the whole torus but are trapped because of the magnetic mirror force if they do not have a high enough velocity parallel to the magnetic field. In order to have trapped electrons the collision frequency needs to be lower than the bounce frequency otherwise the collisions will scatter the particles before they can complete a bounce. As these electrons are trapped on the low field side the curvature drift, the middle term in Eq. (2.14), is not averaged out, as it is for a free particle which travels to the high field side. This is due to the fact that the direction of $\hat{\boldsymbol{b}} \cdot \nabla B$ is always in the same direction if the particle stays on the low field side. As the curvature drift has different directions this will create a charge polarization, giving rise to a ExB-drift

which will strengthen the initial density perturbation. This is the Trapped Electron Mode or TEM. The spatial scales for this is similar as for the ITG-mode.

## 3.3 Transport modeling

In this section we are presenting the models which have been used in the papers.

### 3.3.1 Trapped-gyroLandau-Fluid model

The Trapped-Gyro Landau-Fluid model or TGLF for short is a gyro Landau-fluid model [9] and as such it includes effects that are not present for the fluid model, Landau damping and Finite Larmor Effects. TGLF uses Miller geometry and includes electromagnetic effects. TGLF is a quasi-linear model which by taking moments of the gyrokinetic equations, as described in Sec. (2.7), results in a set of coupled equations. These equations are solved for the linear eigenmodes of the ion and electron temperature gradient (ITG,ETG), trapped ions and electrones modes (TI, TE) and electromagnetic balloning mode (KB modes). A wide spectra for the wavelength is used, including both ion scales ($k_\theta \rho_s < 1$ ) and electron scales ($1 < k_\theta \rho_s < 24$). The saturation level for the TGLF is fitted to a database of nonlinear gyrokinetic simulations. The saturation used in the papers are the latest SAT1 [11, 10].

### 3.3.2 GENE

The GENE-model uses a Eulerian $\delta f$-method to solve the nonlinear gyrokinetic Vlasov equation [22]. GENE solves for the fluctuating part of the distribution function $\delta f(\mathbf{R}, v_\parallel, \mu, t)$, the parallel component of the vector potential, $A_\parallel(\mathbf{x}, t)$, the parallel component of the magnetic field perturbations, $B_\parallel(\mathbf{x}, t)$ and the electrostatic potential $\phi(\mathbf{x}, t)$. The model uses a magnetic field aligned flux coordinate system where x is aligned to the radial coordinate, y the binormal coordinate and z parallel to the magnetic field and it can handle an arbitrary number of ion species. We have used the linearized Landau-Boltzmann operator [24] for the collisionality and in the papers we used a realistic geometry geometry by using an EFIT-file to calculate the magnetic equilibrium.

### 3.3.3 Integrated modeling

In the previous section we discussed specific turbulent transport codes which uses plasma parameters and calculate the particle fluxes, heat fluxes, growthrates of the modes etc. These codes can be used together with other models, such as for heating, magnetic equilibrium, neoclassical transport, to simulate the whole plasma, this is called integrated modeling. Integrated modeling can be used in two ways, interpretative and predictive modeling. Interpretative modeling uses given plasma profiles as input to the codes and calculates a number of different things such as, particle deposition, linear growth rates, particle fluxes etc. Predictive simulations evolve the plasma profiles (n, T, J, $v_{tor}$) in time, self-consistently.

One integrated model which have been used in Paper A, B and C is the JETTO transport code [4]. Experimental profiles are taken from quasi-steady state, where the outward fluxes are in balance with the internal sources, as a starting point and the predictive simulations are evolved in time until they find the theoretical quasi-steady-state. These theoretical quasi-stedy states are compared with the experimental (physical) steady state to asses the validity of the theoretical models. With integrated modeling it is easy to determine the effect in the plasma for external changes (for example increase of the NBI particle source) or internal changes (for example increase of the plasma current).

During the evaluation the turbulent transport is calculated with transport codes such as TGLF consistently as the plasma profiles changes affects the transport codes. JETTO performs these predictive simulations by solving the particle (i.e. continuity) and energy balance equations and evolving it in time. Here as flux surface averaged equations [4]:

$$\frac{\partial}{\partial t}\langle n\rangle + \frac{1}{v'}\frac{\partial}{\partial \rho_t}\left(v'\langle \Gamma^{\rho_t}\rangle\right) = \langle S_n\rangle \tag{3.6}$$

$$\frac{3}{2}\frac{\partial\langle P_j\rangle}{\partial t} + \frac{1}{v'}\frac{\partial}{\partial \rho_t}\left[v'\langle \boldsymbol{q}_i \cdot \boldsymbol{\nabla}\rho_t\rangle\right] = \langle Q_j\rangle \tag{3.7}$$

$S_n$ is the NBI particle source and Q represent the power gain and losses from NBI-particles, electron-ion thermal equilibration, radiation and Ohmic heating. Both $S_n$ and Q is dependent on the radial position and both can be calculated with various degree of accuracy. The NBI particle source can be taken to be static or calculated with Monte-Carlo type of codes such as ASCOT. This can be done at each time step or at time intervals, which is preferable as some of the NBI codes are computational heavy.

## 3.4 Density Peaking

As the densities are limited by the empiric Greenwald limit, to achieve the highest possible energy output, the highest density need to be where the temperature is highest, i.e. the magnetic axis. To achieve this within the Greenwald ratio we want density peaking which yield the highest density at the magnetic axis. This phenomena where a plasma has higher density at the magnetic axis than the top of the pedestal (for a H-mode) is called density peaking and is a current field of research.

The density peaking is determined by two factors, the particle sources and the internal particle transport. Previous work have studied the importance of the particle sources to the density peaking, and the results are inconclusive. Some studies have shown the particle sources to have a high impact [15, 12] while others have shown a low (around 20 % of the density peaking from the particle sources) or negligible impact [13, 14, 5]. Also more recent studies are inconclusive, at JET [18, 8] the particle sources had a large impact on the peaking while other studies at DIII-D [17] and AUG [7] showed a small or negligible contribution. As the density peaking is important for the effectiveness of a future power plant it is imperative to

clarify the relative contributions from the particle sources and internal transport to the density peaking. Density peaking can be defined in two different ways, global or local. Global density peaking describes the normalized density difference between the core and the top of the pedestal. Local density peaking defines the normalized density gradient at a certain radial position in the plasma. We are going to focus on local density peaking and it origins. To quantify local density peaking we will start with the flux surface averaged continuity equation from (3.6):

$$\frac{\partial}{\partial t}\langle n\rangle + \frac{1}{v'}\frac{\partial}{\partial \rho_t}\left(v'\langle \Gamma^{\rho_t}\rangle\right) = \langle S_n\rangle \tag{3.8}$$

Here $\Gamma$ is the particle flux and it can be decomposed into a diffusive and convective part which was shown in Eq. (3.3). The density peaking has two sources, the turbulent transport and the internal particle sources. This can clearly seen by inserting the decomposed particle flux in Eq. (3.8) and assume steady-state.

$$\frac{a}{L_{\langle n_e\rangle}} = -\frac{a\langle|\boldsymbol{\nabla}\rho_t|\rangle^2}{\langle|\boldsymbol{\nabla}\rho_t|^2\rangle}\frac{V^{PB}_{\langle n_e\rangle}}{D^{PB}_{\langle n_e\rangle}} + \frac{a\langle|\boldsymbol{\nabla}\rho_t|\rangle}{v'\langle|\boldsymbol{\nabla}\rho_t|^2\rangle\langle n_e\rangle D^{PB}_{\langle n_e\rangle}}\int_0^{\rho_t} v'\langle S_n\rangle d\rho_t \tag{3.9}$$

Here v' is the the derivative of the plasma volume, $\langle S_n\rangle$ is the particle input from the particle source per flux surface/s. The left hand side is the total local peaking factor for the plasma. The first term on the RHS is the peaking that comes from the turbulent transport. This term is entirely determined by the fraction of the particle balance pinch and diffusion. The second term on the right hand side is the source term and a large particle balance diffusion dampens this term. This can be seen as a discharge with a high particle balance diffusion quickly dispels the particle source. Thus an increase in the particle source will not add to the density peaking of the discharge, in a significant manner. A discharge with high particle balance diffusion can still be peaked through the turbulent transport, if the particle balance pinch is of the same magnitude as the diffusion or larger.

# CHAPTER 4

# BRIEF SUMMARY OF THE PAPERS

The common feature through papers I-IV is the evaluation of the importance of the particle source for the density peaking at current machines in order to understand the extrapolation for future machines.

In Paper I, interpretative and predictive simulations with JETTO for four collisionality scans at JET are presented each with three discharges: Deuterium L-mode with Carbon wall, hydrogen H-mode, deuterium H-mode and deuterium H-mode with high $\beta$. While doing the predictive simulations, the electron density, electron and ion temperature profiles were evolved in time until a quasi-steady state was found. In each collisionality scan important dimensionless parameters are kept constant such as $\beta$, normalized gyroradius, safety factor, magnetic shear, normalized temperature gradients and $Z_{eff}$. To recognize the effect of the NBI-source on the density peaking simulations were performed with and without the NBI particle source (the heating from the NBI-beams were still applied). The simulations were done with JETTO, TGLF was used as transport model. The results showed that the turbulent transport was the major cause of the density peaking for the Carbon wall L-mode while the H-mode discharges showed a high dependency on the NBI-source. As discharges with carbon wall has a higher impurity content these discharges were also simulated with a 2% carbon content which did not affect the density peaking in a significant way.

In paper II, collisionality scans at JET are described in great experimentally detail and analyzed with TGLF and GENE. The perturbative transport coefficients were measured using a gas puffing technique, which involves perturbing the particle density and measuring the rate which the density perturbation moved through the plasma. Transport simulations and experimental measured values both concluded that the NBI fueling had a different impact for the the density peaking between the collisionality scans. It was determined that half of the density peaking came from the NBI fueling for the H-mode discharges and 10% - 20% for the L-mode discharges.

In paper III, a similar collisionality scan was performed at DIII-D. As in Paper II the perturbative transport coefficients were measured using a gas puffing technique and result showed higher values for the low collisionality discharge, both

for the diffusion and pinch. The measured fraction of the pinch and diffusion, which constitutes the turbulent transport contribution to the density peaking, were similar to measured density peaking indicating that the NBI fueling has a small impact on the peaking. Studies were done with TGLF to investigate the most unstable mode and the medium and high collisionality discharge showed a dominant ITG-mode. The low collisionality discharge displayed a TEM as the most unstable mode which might explain the large difference in transport coefficients.

In Paper IV, we focus on the comparison of the particle transport and density peaking between JET and DIII-D. This was done by comparing two H-mode collisionality scans, one at JET and one at DIII-D. The perturbative particle transport coefficients were calculated by performing density gradient scans for the discharges with TGLF. These values were compared with the experimentally measured values which were presented in paper B, for DIII-D, and C, for JET. Particle balance transport coefficients were also calculated and were lower than the perturbative values which suggest that one can not make the assumption that the perturbative and particle balance transport coefficients are equal. The fraction between between the particle balance pinch and diffusion were calculated as its values represent the turbulent transport contribution to the density peaking. Results showed that the DIII-D discharges had the majority of its density peaking due to the turbulent transport while the JET discharges had the largest contribution form the particle source. This conclusion was also supported by linear and non-linear simulations with GENE which calculated the zero flux peaking factor, i.e. the turbulent transport contribution to the density peaking. Sensitivity studies were performed to determine which parameters were responsible for the large difference in the contribution to density peaking from the turbulent transport in DIII-D and JET, the largest impact came from the temperature gradients.

# BIBLIOGRAPHY


[1] P. Bellan. *Fundamentals of Plasma Physics*. Cambridge University Press.

[2] I. Braginskii. *Reviews of Plasma Physics 1*. Consultants Bureau, 1965.

[3] A.J. Brizard and T.S. Hahm. Foundations of nonlinear gyrokinetic theory. *Reviews of modern physics*, 79, 2007.

[4] G. Cennachi and A. Taroni. Jetto: Tech. rep. jet-ir (88) 03 jet reports. 1988.

[5] C. Angioni et al. Particle transport in tokamak plasmas, theory and experiment. *Plasma Phys. Control. Fusion*, 51(124017), 2009.

[6] D'haeseleer, W.D. et. al. *Flux Coordinats and Magnetic Field Structure*. Springer Series in Computational Physics.

[7] E. Fable et al. The role of the source versus the collisionality in predicting a reactor density profile as observed on asdex upgrade discharges. *Nucl. Fusion*, 59(076042), 2019.

[8] F. Eriksson et al. Interpretative and predictive modelling of jet collisionality scans. *Plasma Phys. Control. Fusion*, 61(102487), 2019.

[9] G. Staebler et. al. Gyro-landau fluid equations for trapped and passing particles. *Phys. Plasmas*, 12(102508), 2005.

[10] G. Staebler et. al. The role of zonal flows in the saturation of multi-scale gyrokinetic turbulence. *Phys. Plasmas*, 23(062518), 2016.

[11] G. Staebler et. al. A model of the saturation of coupled electron and ion scale gyrokinetic turbulence. *Nucl. Fusion*, 57(066046), 2017.

[12] Garzotti, L. et al. Simulations of source and anomalous pinch effects on the density profile peaking of jet h-mode plasmas. *Nucl. Fusion*, 46(994), 2006.

[13] H. Weisen et al. Shear and collisionality dependences of particle pinch in jet l-mode plasmas. *Plasma Phys. Control. Fusion*, 46(751), 2004.

[14] M. Maslov et al. Density profile peaking in jet h-mode plasmas: experiments versus linear gyrokinetic predictions. *Nucl. Fusion*, 49(075037), 2009.

[15] M. Valovič et al. On the correlation between density profile and particle flux in h-mode tokamak plasmas and the implication for iter. *Nucl. Fusion*, 47(196), 2007.

[16] P. Mantica et al. Experimental study of the ion critical-gradient length and stiffness level and the impact of rotation in the jet tokamak. *Physical review letters*, 102(175002), 2009.

[17] S. Mordijck et al. Collisionality driven turbulent particle transport changes in diii-d h-mode plasmas. *Nucl. Fusion*, 60(066019), 2020.

[18] T. Tala et al. Density peaking in jet - driven by fuelling or transport? *Nucl. Fusion*, 60(066019), 2020.

[19] R.E. Waltz et.al. Gyrolandau fluid models for toroidal geometry. *Physics of Fluids b: Plasma physics*, 4(3138), 1992.

[20] J. P. Freidbert. *Ideal MHD*. Cambridge University Press.

[21] H. Hopf. Abbildungsklassenn-dimensionaler mannigfaltigkeiten. *Mathematische Annalen*, 96:209–224, 1927.

[22] F. Jenko and W. Dorland. *Plasma Phys. Contr. Fusion*, 43(12A), 2001.

[23] J. Lawson. Some criteria for a power producing thermonuclear reactor. *Poceedings of the Physical Society. Section B*.

[24] F. Merz. *Gyrokinetic simulation of multiomode plasma turbulence*. PhD thesis, Universität Münster.

[25] J. Weiland. *Stability and Transport in Magnetic Confinement Systems*. Springer Series on Atomic, Optical, and Plasma Physics.

[26] J. Wesson. *Tokamaks, Third edition*. Oxford University Press.